RSC Advances

PAPER

View Article Online
View Journal | View Issue

Cite this: *RSC Adv.*, 2020, **10**, 29575

Glycerine-based synthesis of a highly efficient Fe_2O_3 electrocatalyst for N_2 fixation†

Meng Wang, Feifei Li* and Juan Liu

Received 4th July 2020
Accepted 5th August 2020

DOI: 10.1039/d0ra05831a

rsc.li/rsc-advances

The electrochemical nitrogen reduction reaction (NRR) is a promising approach to convert N_2 into high value-added NH_3. However, it is still a challenge to achieve an efficient electrocatalyst for the NRR. Herein, it is demonstrated that the Fe_2O_3 nanoparticles (NPs) generated from a glycerine-based synthesis can be applied as highly efficient catalysts for the NRR. The Fe_2O_3 NPs show good performance with a high NH_3 yield (22 μg mg_{cat}^{-1} h^{-1}) and a favorable Faradaic efficiency (FE) (3.5%) at −0.5 V *vs.* reversible hydrogen electrode (RHE). The facile synthesis strategy and satisfactory electrochemical properties demonstrate the potential application of the as-synthesized Fe_2O_3 NPs for NRR.

1. Introduction

Ammonia (NH_3) is a highly important chemical in many aspects of industrial production and daily life.[1,2] Fixation of N_2 to NH_3 is an important step for the natural N_2 cycle.[3–5] The current synthesis of NH_3 mainly depends on the industrial Haber–Bosch process, which involves serious energy consumption and leads to large amounts of greenhouse gas emissions.[6,7] To realize a green and sustainable strategy for N_2 fixation, electrochemical reduction of N_2 has recently attracted much attention, being an environmentally friendly route involving mild conditions.[8–10]

To date, a number of catalysts have been developed for the NRR, including noble metals,[11–13] transition metals,[14,15] metal-free materials,[16–18] metal–C composite materials[19–21] and Au–Fe_3O_4.[22] These catalysts have demonstrated potential applications in the NRR with improved FE and NH_3 yield. Most of the catalysts were synthesized with the assistance of surfactants (structure-directing agents) through solution methods.[23] However, the surfactants could passivate the catalyst surface, which decreases the activity of the catalyst since the reactions take place on the catalyst surface. Therefore, the catalyst with a clean surface could be very important for achieving the high activity.

Herein, we successfully synthesized the clean-surface Fe_2O_3 electrocatalyst for NRR by using glycerine as solvent with a subsequent calcination process. There was no need of surfactants in the synthesis process and the particles were further calcinated, guaranteeing the clean nature of the Fe_2O_3 surface. The as-prepared Fe_2O_3 NPs demonstrated a good electrocatalytic performance for NRR, with a high NH_3 yield (22 μg mg_{cat}^{-1} h^{-1}) and a favorable FE (3.5%) at −0.5 V *vs.* reversible hydrogen electrode (RHE).

2. Materials and reagents

Glycerine ($C_3H_8O_3$) (purity, 99.5%), iron(III) nitrate nonahydrate ($Fe(NO_3)_3 \cdot 9H_2O$) (purity, 98.5%) and ethanol (CH_3CH_2OH) (purity ≥ 98.5%) were purchased from Sinopharm Chemical Reagent Co. Ltd.

2.1. Synthesis of Fe_2O_3 nanoparticles (NPs)

121.2 mg of iron(III) nitrate nonahydrate was added into 5 mL glycerin. Then the solution was ultrasonicated for 10 min. The uniform solution was transferred into the Teflon-lined stainless-steel autoclave and heated at 180 °C for 20 h. The obtained product washed with ethanol and water for three times and dried at room temperature for 12 h. Then the product was put into a tubular furnace, heated to 450 °C for 2 h at the heating rate of 10 °C min^{-1} under air. Finally, Fe_2O_3 NPs was obtained.

2.2. Characterization

A Rigaku Dmax-rc X-ray diffractometer was used to perform X-ray diffraction (XRD) characterization. The transmission electron microscopy (TEM) images were obtained on a JEM 1400 TEM instrument. The X-ray photoelectron spectroscopy (XPS) characterization was conducted with ESCALAB 250.

2.3. Electrode preparation

5 mg as-obtained Fe_2O_3, 40 μL Nafion (5% wt) and 960 μL ethanol were mixed by ultrasound for forming suspension. 50 μL suspension was modified on 1 × 1 cm carbon cloth (CC). The Fe_2O_3–CC was used as working electrode.

Kangda College of Nanjing Medical University, Lianyungang, 222000, China. E-mail: ffl@foxmail.com

† Electronic supplementary information (ESI) available. See DOI: 10.1039/d0ra05831a

2.4. Electrochemical reduction of N_2

Electrochemical reduction of N_2 was carried out in a typical three-electrode gastight two-compartment reaction vessel separated by an anion exchange membrane (Nafion 211) on a CHI760 electrochemical workstation (Chenhua, Shanghai). The experiment was performed in 0.1 M Na_2SO_4 solution (50 mL each compartment). A Pt wire was used as the counter electrode and an Ag/AgCl (4.0 M KCl) was used as reference. All potentials were converted to RHE. The electrolyte was then purged with N_2 for at least 30 min. N_2 was delivered into the cathodic compartment at a constant rate of 20 mL min^{-1}. The potentiostatic tests were performed in 0.1 M Na_2SO_4 aqueous solution at different potentials such as −0.3, −0.4, −0.5, −0.6, and −0.7 V *vs.* RHE. The NH_3 yields and FEs of products were calculated as follows:

$$NH_3 \text{ yields } (\mu g\ mg_{cat}^{-1}\ h^{-1}) = m/(t \times m_{cat}) \quad (1)$$

$$FE\ (\%) = \alpha mF/MQ \quad (2)$$

where m is the mass of NH_3, m_{cat} is the mass of catalyst, α is the quantity of transferred electrons for producing NH_3, M is the relative molecular mass, and Q is the total quantity of the electric charge.

2.5. Determination of NH_3 and N_2H_2

The detections of NH_3 and N_2H_2 were made by indophenol blue and Watt–Chrisp methods, respectively, according to the reported literature.[24]

3. Results and discussion

The Fe_2O_3 electrocatalysts were synthesized by using glycerine as the solvent with a subsequent calcination process. In the synthesis system, there was no surfactant and the particles were further calcinated. Therefore, the Fe_2O_3 particles with clean surface could be obtained by our present synthetic route. Fig. 1(a) shows the X-ray diffraction (XRD) pattern of the as-synthesized Fe_2O_3, which agrees well with the JCPDS No. 33-0664. This demonstrates the successful formation of Fe_2O_3. Low peak intensity may be caused by small size of Fe_2O_3 particles. Transmission electron microscopy (TEM) images of the Fe_2O_3 suggests that the diameters of as-synthesized Fe_2O_3 nanoparticles are in the range of 4–6 nm (Fig. 1(b) and (c)).

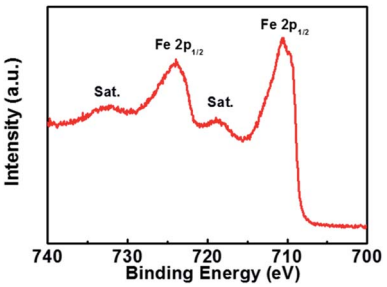

Fig. 2 High resolution XPS spectrum of Fe 2p.

To investigate the surface elemental state of Fe_2O_3 NPs, we analyzed the chemical states of the Fe_2O_3 NPs by XPS analysis. There are two Fe^{3+} peaks located at 711.8 eV and 725.3 eV, corresponding to Fe $2p_{1/2}$ and Fe $2p_{3/2}$,[25] agreeing well with Fe_2O_3 NPs (Fig. 2). The XPS spectrum result further demonstrated the successful synthesis of Fe_2O_3 NPs.

The synthesized Fe_2O_3 NPs were then used as the electrocatalysts for the electrochemical nitrogen reduction reaction (NRR). The produced ammonia was analyzed and quantified based on the indophenol blue method. Before NRR experiment, the corresponding calibration curve for ammonia by indophenol blue method was first determined and shown in Fig. 3.

The N_2-fed electrolytes in 0.1 M Na_2SO_4 electrolytes at different potentials for 2 h were mixed with the indophenol reagent, and their absorbance changed at 660 nm were depicted in Fig. 4(a). It indicated the substantial electroreduction of inert N_2 into valuable NH_3 was achieved using the as-synthesized Fe_2O_3 electrocatalyst. Fig. 4(b) presented the chronoamperometric curves as a function of reaction time at varying applied potentials in 0.1 M Na_2SO_4, demonstrating the Fe_2O_3 nanoparticles have good stability for NRR from −0.3 V to −0.6 V. The average NH_3 yield and the corresponding Faradaic efficiency (FE) was given in Fig. 4(c), in which the favorable NH_3 yield was 22.0 μg mg_{cat}^{-1} h^{-1} with FE value of 3.5% at −0.5 V. The NRR performance of the as-synthesized Fe_2O_3 is comparable to lots of the NRR electrocatalysts (Table S1†). Therefore, the present synthesized Fe_2O_3 with clean surface might be as a potential catalyst for electrochemical NRR in consideration that there are

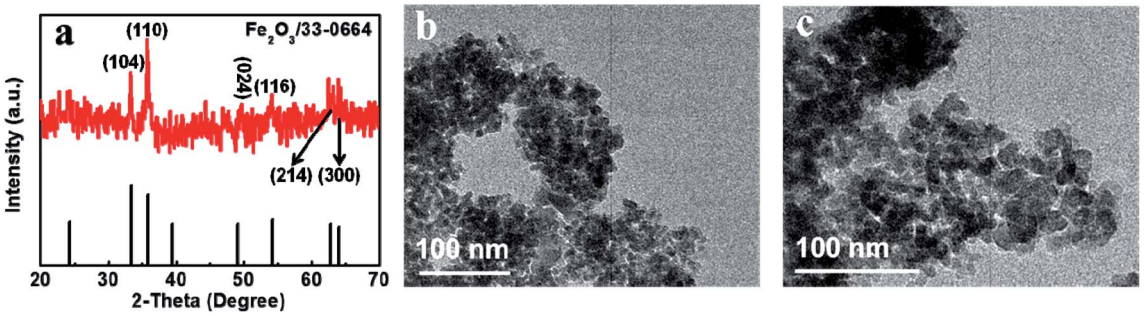

Fig. 1 (a) XRD pattern and (b and c) TEM images of the Fe_2O_3 after calcination at 450 °C.

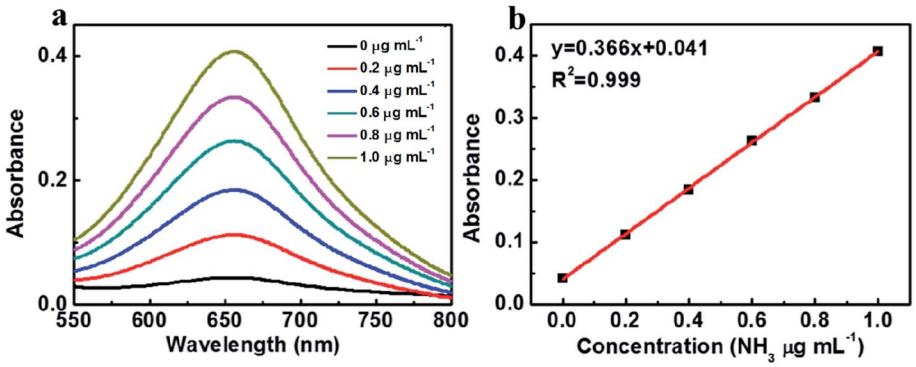

Fig. 3 (a) UV-vis absorption spectra of different concentration ammonia in 0.1 M Na_2SO_4 solution, (b) standard curve of ammonia in 0.1 M Na_2SO_4 solution.

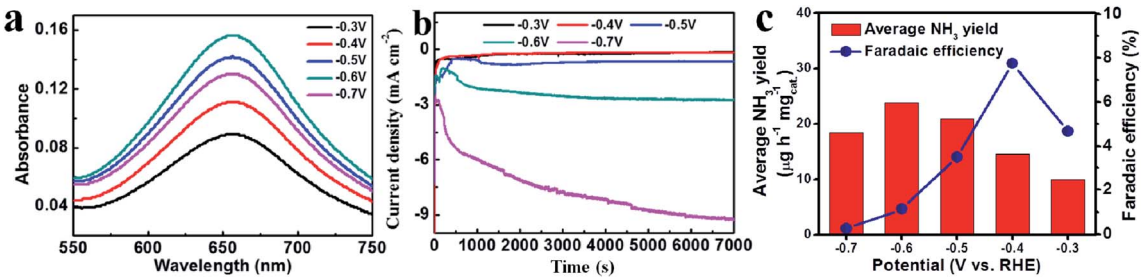

Fig. 4 UV-vis absorption spectra in (a) 0.1 M Na_2SO_4 electrolytes stained with the indophenol indicator after NRR electrolysis at a series of potentials for 2 h, (b) time-dependent current density curves for Fe_2O_3 at different potentials in 0.1 M Na_2SO_4 solution, (c) NH_3 yields and FEs for Fe_2O_3 at a series of potentials in 0.1 M Na_2SO_4.

abundant Fe element in the earth. TEM image of catalyzed Fe_2O_3 was tested after nitrogen fixation at −0.5 V. It was found that the morphology did not changed significantly, which indicated the good stability of the as-synthesized Fe_2O_3 (Fig. S1†).

The NNR performance is highly related to the electrochemically active surface area (ECSA). Therefore, the ECSA of the as-prepared Fe_2O_3 was further studied. Here, the ECSA was reflected by double layer capacitance (C_{dl}) since there was a linear proportional relationship between ECSA and C_{dl}, which could be obtained by cyclic voltammetry curves in the range of 0.1–0.2 V (Fig. 5(a)). Based on Fig. 5(b), the high C_{dl} of 1.6 mF cm^{-2} (Fig. 5(b)) further demonstrated that Fe_2O_3 had high ECSA for NRR.

The hydrazine byproduct was further determined through a Watt–Chrisp method. Fig. 6(a) showed the corresponding calibration curve based on UV-vis absorption at 455 nm. As shown in Fig. 6(b), the by-product of hydrazine was not detected, implying the high selectivity of Fe_2O_3 for NH_3 production (Fig. 6). Hence, the as-prepared Fe_2O_3 catalyst could be used as a high-selective catalyst for producing NH_3 by electrochemical NRR.

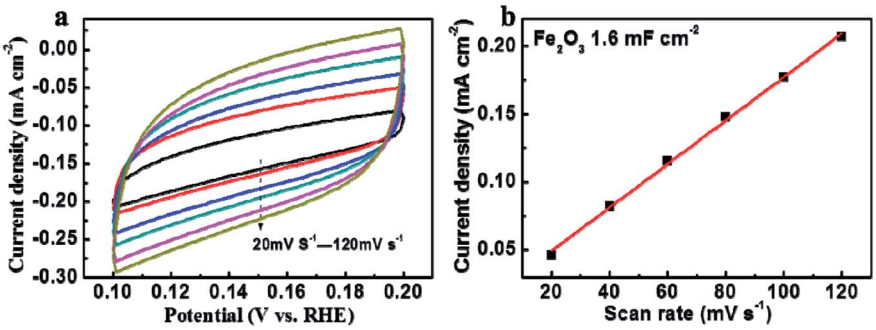

Fig. 5 (a) Cyclic voltammetry curves of Fe_2O_3 at different scanning rate of potential in 0.1 M Na_2SO_4 solution, (b) the double-layer capacitance of Fe_2O_3.

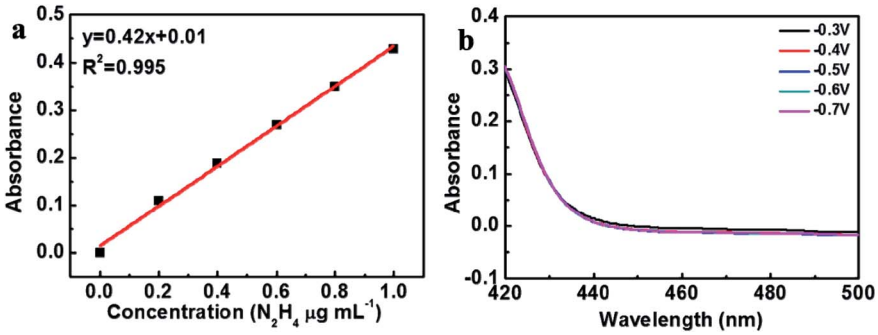

Fig. 6 (a) Standard curve of hydrazine in 0.1 M Na_2SO_4 solution, (b) UV-vis absorption spectra of hydrazine in 0.1 M Na_2SO_4 electrolytes after NRR electrolysis at a series of potentials for 2 h.

We also explored the NRR performance of Fe_2O_3 in 0.1 M KOH. The selected potential was −0.5 V. Unfortunately, the current density declined rapidly within 2 h (Fig. S2†).

4. Conclusions

In summary, Fe_2O_3 synthesized by glycerine-based route with subsequent calcination process can be adopted as highly efficient NRR catalysts. Thanks to the clean surface of the catalyst, the Fe_2O_3 NPs exhibited good performance with a 22 μg mg_{cat}^{-1} h^{-1} NH_3 yield and a 3.5% Faraday efficiency at −0.5 V for NH_3 production, which outperformed lots of the previous catalysts. The flexible strategy and the good electrochemical performance endow Fe_2O_3 with potential application in NRR.

Conflicts of interest

The authors declare that they have no known competing financial interests or personal relationships that could have appeared to influence the work reported in this paper.

Acknowledgements

The research was supported by Science and technology development foundation, Nanjing Medical University, China (No. NMUB2019273).

References

1 J. G. Chen, R. M. Crooks, L. C. Seefeldt, K. L. Bren, R. M. Bullock, M. Y. Darensbourg, P. L. Holland, B. Hoffman, M. J. Janik, A. K. Jones, M. G. Kanatzidis, P. King, K. M. Lancaster, S. V. Lymar, P. Pfromm, W. F. Schneider and R. R. Schrock, *Science*, 2018, **360**, 6391–6398.
2 M. Van Damme, L. Clarisse, S. Whitburn, J. Hadji-Lazaro, D. Hurtmans, C. Clerbaux and P. F. Coheur, *Nature*, 2018, **564**, 99–103.
3 Y. Song, D. Johnson, R. Peng, D. K. Hensley, P. V. Bonnesen, L. Liang, J. Huang, F. Yang, F. Zhang, R. Qiao, A. P. Baddorf, T. J. Tschaplinski, N. L. Engle, M. C. Hatzell, Z. Wu, D. A. Cullen, H. M. Meyer, B. G. Sumpter and A. J. Rondinone, *Sci. Adv.*, 2018, **4**, 1700336–1700344.
4 J. S. Anderson, J. Rittle and J. C. Peters, *Nature*, 2013, **501**, 84–87.
5 J. W. Erisman, M. A. Sutton, J. Galloway, Z. Klimont and W. Winiwarter, *Nat. Geosci.*, 2008, **1**, 636–639.
6 V. Smil, *Nature*, 1999, **400**, 415.
7 B. M. Hoffman, D. Lukoyanov, Z. Y. Yang, D. R. Dean and L. C. Seefeldt, *Chem. Rev.*, 2014, **114**, 4041–4062.
8 X. Cui, C. Tang and Q. Zhang, *Adv. Energy Mater.*, 2018, **8**, 1800369–1800394.
9 X. Wang, Q. Zhang, X. Zhang, C. Wang, Z. Xie and Z. Zhou, *Small Methods*, 2019, **3**, 1800334–1800339.
10 Q. Hao, C. W. Liu, G. H. Jia, Y. Wang, H. Arandiyan, W. Wei and B. J. Ni, *Mater. Horiz.*, 2020, **7**, 1014–1029.
11 Z. Geng, Y. Liu, X. Kong, P. Li, K. Li, Z. Liu, J. Du, M. Shu, R. Si and J. Zeng, *Adv. Mater.*, 2018, **30**, 1803498–1803504.
12 J. Wang, L. Yu, L. Hu, G. Chen, H. Xin and X. Feng, *Nat. Commun.*, 2018, **9**, 1795–1802.
13 C. Y. Yang, B. L. Huang, S. X. Bai, Y. G. Feng, Q. Shao and X. Q. Huang, *Adv. Mater.*, 2020, **32**, 2001267–2001277.
14 X. M. Hu, S. Y. Guo, S. L. Zhang, X. Y. Guo, Y. F. Li, S. P. Huang, K. Zhang and J. W. Zhu, *J. Mater. Chem. A*, 2019, **7**, 25887–25893.
15 Y. T. Liu, X. X. Chen, J. Y. Yu and B. Ding, *Angew. Chem., Int. Ed.*, 2019, **58**, 18903–18907.
16 W. H. Kong, R. Zhang, X. X. Zhang, L. Ji, G. S. Yu, T. Wang, Y. L. Luo, X. F. Shi, Y. H. Xu and X. P. Sun, *Nanoscale*, 2019, **11**, 19274–19277.
17 H. Zou, W. Rong, B. Long, Y. Ji and L. Duan, *ACS Catal.*, 2019, **9**, 10649–10655.
18 Y. Liu, Q. Li, X. Guo, X. Kong, J. Ke, M. Chi, Q. Li, Z. Geng and J. Zeng, *Adv. Mater.*, 2020, **32**, 1907690–1907697.
19 H. Cheng, P. X. Cui, F. R. Wang, L. X. Ding and H. H. Wang, *Angew. Chem., Int. Ed.*, 2019, **58**, 15541–15547.
20 H. T. Xie, Q. Geng, X. J. Zhu, Y. L. Luo, L. Chang, X. B. Niu, X. F. Shi, A. M. Asire, S. Y. Gao, Z. M. Wang and X. P. Sun, *J. Mater. Chem. A*, 2019, **7**, 24760–24764.
21 B. Yu, H. Li, J. White, S. Donne, J. B. Yi, S. B. Xi, Y. Fu, G. Henkelman, H. Yu, Z. L. Chen and T. Y. Ma, *Adv. Funct. Mater.*, 2019, **30**, 1905665–1905676.

22 J. Zhang, Y. J. Ji, P. T. Wang, Q. Shao, Y. Y. Li and X. Q. Huang, *Adv. Funct. Mater.*, 2019, **30**, 1906579–1906587.
23 X. Yang, L. Chen, Y. Li, J. C. Rooke, C. Sanchez and B. Su, *Chem. Soc. Rev.*, 2017, **46**, 481–558.
24 C. Zhang, S. Liu, T. Chen, Z. Li and J. Hao, *Chem. Commun.*, 2019, **55**, 7370–7373.
25 X. Huang, M. Lu, X. Zhang, G. Wen, Y. Zhou and L. Fei, *Scr. Mater.*, 2012, **67**, 613–616.